

Stable Thiolate Adducts of $\text{Rh}_2(\text{OAc})_4$ – Assembly of Hexametallic Ni_4Rh_2 Complexes

Sara Schmorl,^a Martin Börner, and Berthold Kersting^{a,*}

^a *Institut für Anorganische Chemie, Universität Leipzig, Johannisallee 29, 04103 Leipzig, Germany*, E-mail: b.kersting@uni-leipzig.de Fax: +49(0)341-97-36199

Supporting Information

Contents

- 1) Synthetic Procedures and Characterization Details
- 2) X-ray Crystallography
- 3) Characterization of **2** by Squid Magnetometry

1. Synthetic Procedures and Characterization Details

Materials and methods: The nickel complex $[\text{Ni}_2\text{L}(\mu\text{-F})](\text{ClO}_4)$ **1** was prepared according to the literature procedures.¹ All reagents and solvents were commercial grade and used without further purification. Metal complexes were synthesized under a protective atmosphere of argon unless stated otherwise. Melting points were recorded with an Electrothermal IA9000 series instrument using open glass capillaries and are uncorrected. Mid (4000–400 cm^{-1}) infrared spectra (4 cm^{-1} resolution) were taken on a BRUKER TENSOR 27 FT-IR spectrophotometer. UV-vis spectra were measured on a Jasco V-670 UV-vis/near-IR spectrophotometer in 1 cm quartz cells (Hellma). Elemental analyses were determined on a Vario EL element analyzer (Elementar Analysensysteme GmbH, Hanau). Temperature-dependent magnetic susceptibility measurements were performed on a MPMS 7XL SQUID device (Quantum Design) in the temperature range 2–330K at an applied magnetic field of 0.5 T. The observed susceptibility data were corrected for underlying diamagnetism using Pascals's constants. Mass spectra were obtained using the positive ion electrospray ionization modus (ESI) on a Bruker Daltronics ESQUIRE 3000 Plus ITMS or Impact II UHR Qq-TOF instrument. Diffuse UV-vis reflectance measurements were conducted on a Jasco V-670

UV-vis-NIR spectrophotometer equipped with an ARN-914 absolute reflectance measurement unit. Because of strong absorbance, the samples were optically diluted with BaSO₄ (~ 99 wt%), the baseline being recorded with a Spectralon white standard. The diffuse reflectance (R) of the sample was converted to absorbance (T) via the Kubelka-Munk function: $T = (1-R)^2/(2R)$ implemented in the spectramanager software.

Caution! *Perchlorate salts of transition-metal complexes are hazardous and may explode. Only small quantities should be prepared and great care should be taken when handling these salts.*

[{LNi₂(μ-F)}₂{Rh₂(OAc)₄}]₂(ClO₄)₂·8H₂O (2). To a solution of **1** (100 mg, 0.11 mmol, 1.0 eq.) in MeCN (30 ml) was added a solution of Rh₂(OAc)₄(H₂O)₂ (105.6 mg, 0.22 mmol, 2.0 eq.) in MeCN (5 ml). The mixture was stirred for further 12 h at r.t. after which ethanol (40 mL) was added. The solution was evaporated under reduced pressure until incipient precipitation and left to stand for another 2 h. The resulting green solid was isolated by filtration and washed with cold ethanol. The crude product was purified by recrystallization from a mixed MeCN/EtOH solvent system and dried in vacuum. Dark green microcrystalline solid. Yield: 74 mg (32.9 mmol, 30 %). M.p. 307 °C. Elemental analysis for C₈₄H₁₄₀Cl₂F₂N₁₂Ni₄O₁₆Rh₂S₄·8H₂O (2251.83+162.14) calcd: C 41.79, H 6.60, N 6.96 %; found C 41.78, H 6.09, N 6.80 %. *m/z* (ESI+, CH₃CN): 2149.4 [M-ClO₄]⁺, 1247.4 [M-{(Ni₂L(μ-F))⁺-2ClO₄}]⁺. IR (KBr): ν/cm^{-1} = 3442 (m), 3272 (m), 2952 (s), 2926 (m), 2864 (s), 2814 (m), 1630 (w), 1594 (s, $\nu(\text{OAc}^-)$), 1437 (s), 1362 (m), 1300 (m), 1282 (m), 1228 (m), 1188 (w), 1157 (m), 1120 (s), 1107(m), 1088 [s, $\nu(\text{ClO}_4^-)$], 1054 (m), 1015 (w), 1004 (w), 981 (m), 944 (w), 923 (w), 870 (s), 850 (w), 816 (w), 746 (w), 698 (m), 625 [s, $\nu(\text{ClO}_4^-)$], 549 (w), 497 (w). UV-vis (CH₂Cl₂/MeOH, 1:1): $\lambda_{\text{max}}/\text{nm}$ ($\epsilon/\text{M}^{-1}\cdot\text{cm}^{-1}$) = 196 (140290), 283 (26930), 319 (22970), 555 (380), 633 sh (267), 1013 (152).

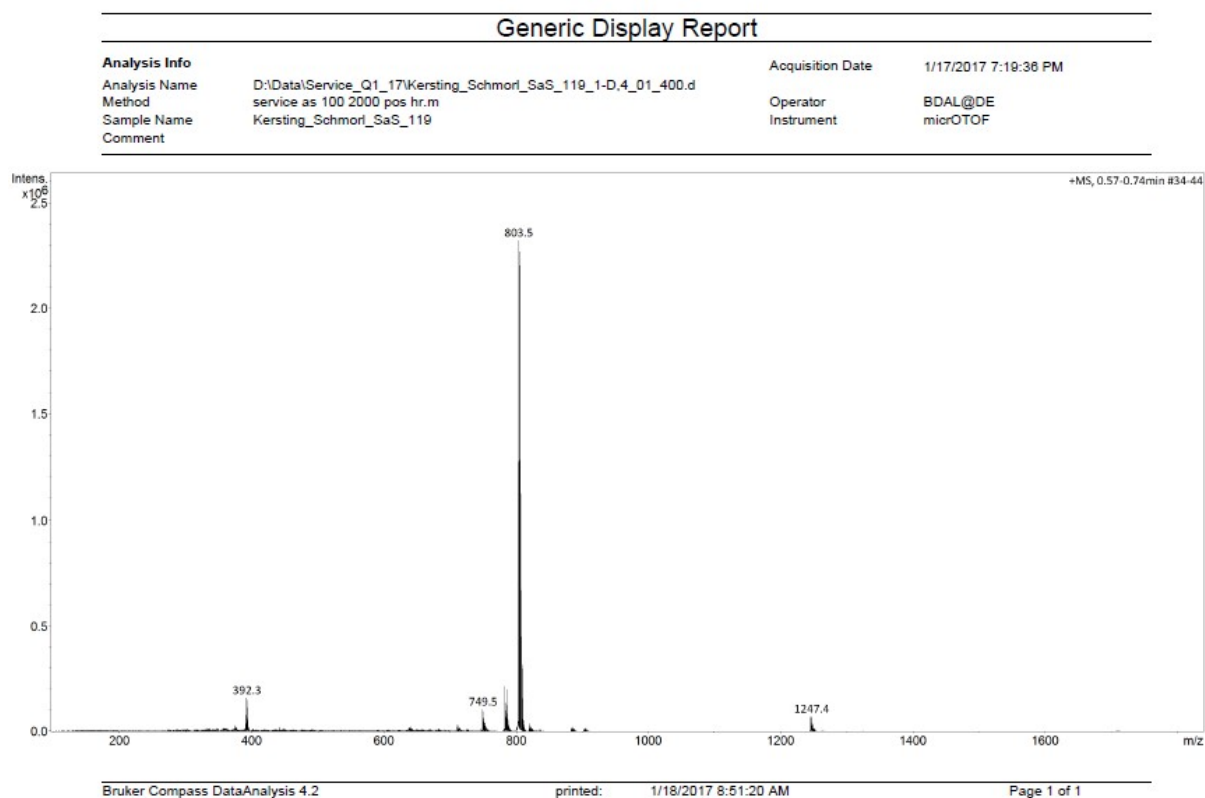


Figure S1. ESI-MS spectrum for $[\{\text{LNi}_2(\mu\text{-F})\}_2(\text{Rh}_2(\text{OAc})_4)](\text{ClO}_4)_2$ in MeCN ($c \sim 10^{-3}$ M). The strong peaks at $m/z = 392.2$ and 803.5 are due to the $[\text{LNi}^{\text{II}}\text{Ni}^{\text{III}}]^{2+}$ dication and the $[\text{LNi}^{\text{II}}_2(\mu\text{-F})]^+$ cation, respectively, which presumably form by decomposition of adduct **2** under the ESI MS experiment.

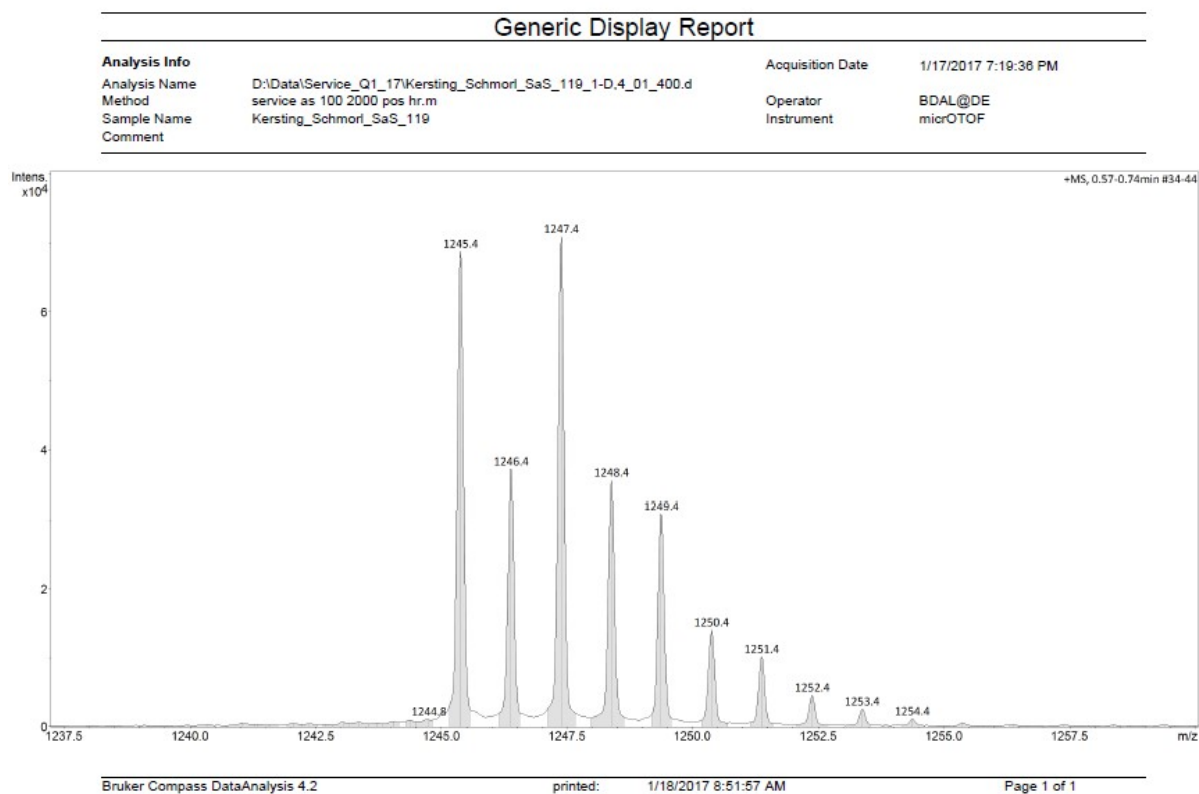


Figure S2. Section of the ESI-MS spectrum for $[\{\text{LNi}_2(\mu\text{-F})\}_2(\text{Rh}_2(\text{OAc})_4)](\text{ClO}_4)_2$ (**2**) ($c \sim 10^{-3}$ M in MeCN). This peak can be assigned to the monoadduct $[\{\text{LNi}^{\text{II}}\text{Ni}^{\text{II}}(\mu\text{-F})\}(\text{Rh}_2(\text{OAc})_4)]^+$.

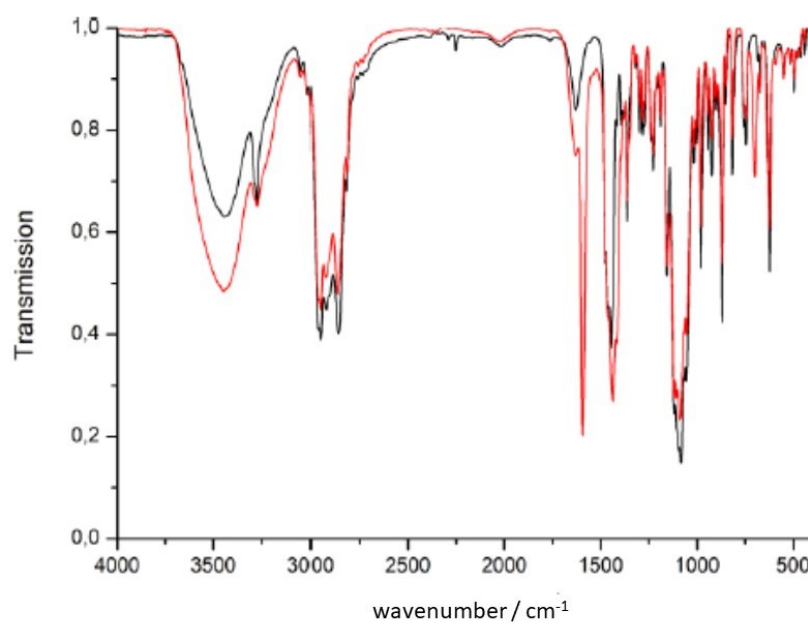


Figure S3. Overlay of the IR spectra of $[\{\text{LNi}_2(\mu\text{-F})\}_2(\text{Rh}_2(\text{OAc})_4)]\text{ClO}_4$ (**2**, red spectrum) and $[\text{LNi}_2(\mu\text{-F})]\text{ClO}_4$ (**1**, black spectrum).

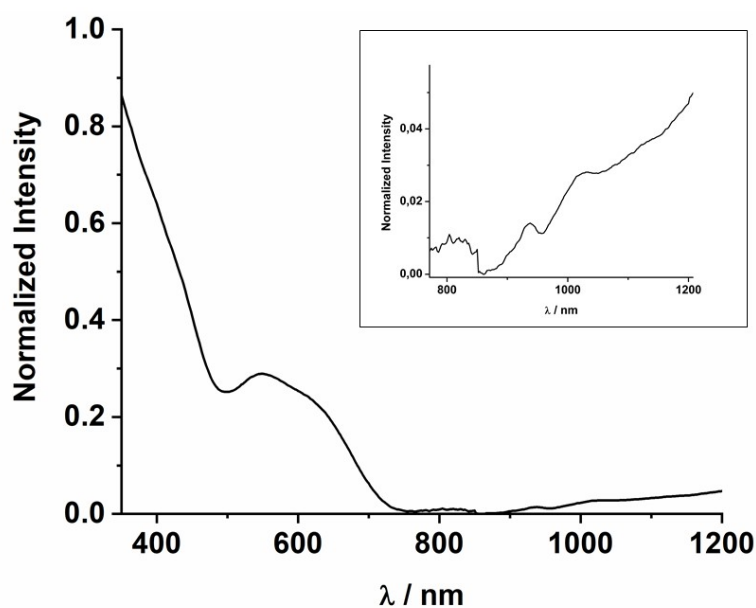


Figure S4. Kubelka-Munk converted diffuse reflectance UV-vis spectrum for **2** (~ 1 wt% finely dispersed in BaSO_4 powder) at 298 K. The inset shows the 800-1200 nm region (note the larger scale). The weak feature at ~ 1020 nm should correspond to the ν_1 transition (${}^3\text{A}_{2g} \rightarrow {}^3\text{T}_{2g}$) of the Ni^{2+} ion in **2**.

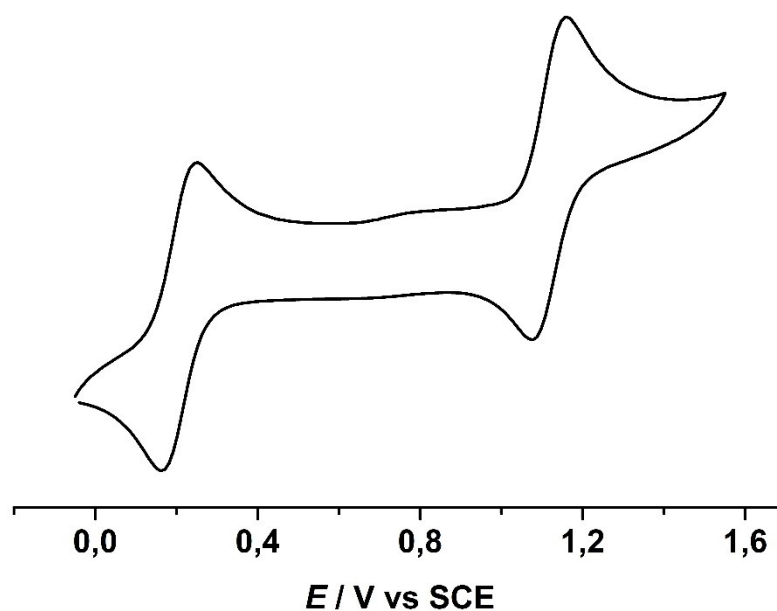


Figure S5. Cyclic voltammogram of **1** in CH_2Cl_2 ($c \sim 10^{-3}$ M, 0.1 M NBu_4PF_6 , Pt disk working electrode, Ag wire reference electrode, scan rate 100 mV/s).

2. X-ray crystallography. Crystals of 2·5.5DMF suitable for X-ray crystallography were obtained from a mixed MeCN/EtOH/DMF solvent system. Single-crystal X-ray diffraction data were collected at 180(2) K on a STOE STADIVARI X-ray diffractometer equipped with an X-ray microsource (Cu-K α , $\lambda = 1.54186 \text{ \AA}$), a multi-layer mirror and a Dectris Pilatus-300K detector. Data processing was carried out with the STOE X-Area software including a spherical absorption correction and scaling routine.² The structures were solved with SHELXT 2018/2³ using dual methods and refined by full matrix least squares minimization on F^2 using version 2018/3 SHELXL⁴ and Olex2.⁵ The coordinates of all non-hydrogen and non-disordered atoms were refined with anisotropic thermal parameters. PLATON was used to search for higher symmetry.⁶ All non-hydrogen atoms were refined anisotropically. H atoms were placed in calculated positions and treated isotropically using the 1.2-fold U_{iso} value of the parent atom except methyl protons, which were assigned the 1.5-fold U_{iso} value of the parent C atoms. The coordinates of all non-hydrogen and non-disordered atoms were refined with anisotropic thermal parameters. Graphics were produced with Ortep3⁷ for Windows and PovRAY.^{8,9} One ClO $_4^-$ ion was found to be disordered over two sites. A split atom model was applied to account for this disorder to give site occupancy factors of 0.61/0.39. Four DMF molecules could be refined in this structure. However, this model still exhibits potential solvent accessible void volume (1356 \AA^3 , electron count: 256 electrons). This suggest that ~ 1.5 extra DMF solvates are present giving a total of 5.5 DMF molecules per formula unit.

Crystallographic data for 2: C $_{96}$ H $_{168}$ Cl $_2$ F $_2$ N $_{16}$ Ni $_4$ O $_{20}$ Rh $_2$ S $_4$, $M_r = 2543.25 \text{ g/mol}$, monoclinic, $P2_1/c$, $a = 25.5460(2) \text{ \AA}$, $b = 18.1249(1) \text{ \AA}$, $c = 27.9275(2) \text{ \AA}$, $\beta = 108.378(1)^\circ$, $V = 12271.4(2) \text{ \AA}^3$, $Z = 4$, $\rho_{\text{calcd}} = 1.377 \text{ g/cm}^3$, $T = 180(2) \text{ K}$, $\mu(\text{Cu K}\alpha) = 4.39 \text{ mm}^{-1}$, 147300 reflections measured, 23253 unique, 18645 with $I > 2\sigma(I)$. Final $R_1 = 0.0462$, $wR_2 = 0.1300$ ($I > 2\sigma(I)$), 1385 parameters / 361 restraints, min./max. residual electron density = $-0.78/1.10 \text{ e/\AA}^3$. CCDC-number: 2114853.

3) Characterization of compound 2 by variable temperature dc magnetic susceptibility measurements

The temperature dependence of the magnetic susceptibility of compound 2 was investigated in the temperature range between 2 and 330 K in an applied external field of $B = \mu_0 H = 0.5 \text{ T}$ using an MPMS 7XL SQUID magnetometer (Quantum Design). The observed susceptibility data were corrected for underlying diamagnetism. Figure 4 (main manuscript) shows the experimental data and the theoretical fit in the form of a μ_{eff} versus T plot.

The temperature dependence of the magnetic susceptibility for the Ni₄Rh₂ complex was analysed by using the spin-Hamiltonian (equation S1) by using a full-matrix diagonalization approach.

$$\begin{aligned} \hat{H} = & -2J_1 (\hat{S}_1\hat{S}_2 + \hat{S}_3\hat{S}_4) - 2J_2 (\hat{S}_1\hat{S}_4 + \hat{S}_2\hat{S}_3) \\ & + \sum_{i=1}^4 [D_i (\hat{S}_{zi}^2 - \frac{1}{3} \hat{S}_i (\hat{S}_i + 1)) + g_i \mu_B \hat{S}_{i\tau} B_\tau] \quad (\tau = x, y, z) \end{aligned} \quad (\text{S1})$$

In this model J_1 represents the exchange interaction between the Ni²⁺ ions (S_i , $i = 1-4$) within the dinuclear subunit, whereas J_2 describes the interaction across the Rh₂⁴⁺ core. The D and g values are assumed to be identical for all of the four Ni²⁺ ions. D represents an effective zero-field splitting parameter, and the zero-field splitting tensors of all Ni²⁺ ions are assumed to be collinear. The least-squares fitting of the experimental data over the full temperature range led to $J_1 = +5.9(1)$ cm⁻¹, $J_2 = 0.0$ cm⁻¹, $g = 2.23$, $D = 21.76$ cm⁻¹, and TIP = 172×10^{-6} cm³mol⁻¹. The inclusion of the D parameter improves the low-temperature fit significantly, but is not physically meaningful since temperature dependent magnetic susceptibility measurements are not very appropriate for the determination of the sign and magnitude of D .

Overall, this analysis establishes that magnetic exchange interactions via the Rh₂⁴⁺ core are not significant. In other words, the magnetic properties are solely based on the exchange couplings in the binuclear [Ni₂L(μ -F)]⁺ subunits. The J and g values are in excellent agreement with those reported for other dinuclear nickel(II) complexes of (L)²⁻ providing further support for the absence of significant interdimer exchange coupling in **2**.

There has been much interest in the distance-dependence of superexchange interactions between paramagnetic transition metal ions bridged by extended spacer ligands. Thus, a large number of paramagnetic metal complexes with separations of 5 to 15 Å between the spin centers have been prepared and their magnetic properties have been determined. The magnetic exchange interactions decrease rapidly with increasing separations and the experimentally determined J values approach the values predicted by the Coffman-Buettner relation ($|J| \leq 1$ cm⁻¹ for $d(\text{M}\cdots\text{M}) \geq 9$ Å).¹⁰ The observations made for the nickel(II) complexes presented herein are in good agreement with the reported trend.

References

- 1 A. Jeremies, U. Lehmann, S. Gruschinski, F. Schleife, M. Meyer, V. Matulis, O. A.

- Ivashkevich, M. Handke, K. Stein, B. Kersting, *Inorg. Chem.* **2015**, *54*, 3937-3950.
- 2 Stoe & Cie GmbH, *X-AREA*, *X-RED32*, *X-SHAPE* and *LANA*. Stoe&Cie, Darmstadt, Germany, **2019**.
- 3 G. M. Sheldrick, *Acta Cryst.* **2015**, *A71*, 3-8.
- 4 G. M. Sheldrick, *Acta Cryst.* **2015**, *C71*, 3-8.
- 5 O. V. Dolomanov, L. J. Bourhis, R. J. Gildea, J. A. K. Howard, H. Puschmann, *J. Appl. Cryst.* **2009**, *42*, 339-341.
- 6 A. L. Spek, *PLATON - A Multipurpose Crystallographic Tool*; Utrecht University, Utrecht, The Netherlands, 2000.
- 7 L. J. Farrugia, ORTEP-3 for Windows – a version of ORTEP-III with a graphical user interface. *J. Appl. Cryst.* **1997**, *30*, 565.
- 8 C. Cason, T. Froehlich, N. Kopp, R. Parker, POV-Ray for Windows, version 3.6.2msvc9.win64.
- 9 L. J. Farrugia, *J. Appl. Cryst.* **1997**, *30*, 565.
- 10 R. E. Coffman, G. R. Buettner, *J. Phys. Chem.* **1979**, *83*, 2387–2392